Comput Mech (2014) 53:1183–1196
DOI 10.1007/s00466-013-0959-z

ORIGINAL PAPER

Computational modeling of hypertensive growth in the human carotid artery

Pablo Sáez · Estefania Peña · Miguel Angel Martínez · Ellen Kuhl

Received: 12 August 2013 / Accepted: 7 December 2013 / Published online: 19 December 2013

Abstract Arterial hypertension is a chronic medical condition associated with an elevated blood pressure. Chronic arterial hypertension initiates a series of events, which are known to collectively initiate arterial wall thickening. However, the correlation between macrostructural mechanical loading, microstructural cellular changes, and macrostructural adaptation remains unclear. Here, we present a microstructurally motivated computational model for chronic arterial hypertension through smooth muscle cell growth. To model growth, we adopt a classical concept based on the multiplicative decomposition of the deformation gradient into an elastic part and a growth part. Motivated by clinical observations, we assume that the driving force for growth is the stretch sensed by the smooth muscle cells. We embed our model into a finite element framework, where growth is stored locally as an internal variable. First, to demonstrate the features of our model, we investigate the effects of hypertensive growth in a real human carotid artery. Our results agree nicely with experimental data reported in the literature both qualitatively and quantitatively.

Keywords Biomechanics · Growth · Smooth muscle cells · Hypertension · Finite element method

P. Sáez · E. Peña · M. A. Martínez
Group of Applied Mechanics and Bioengineering, Aragón Institute of Engineering Research, University of Zaragoza, Zaragoza, Spain

P. Sáez · E. Peña · M. A. Martínez
Centro de Investigación Biomédica en Red en Bioingeniería, Biomateriales y Nanomedicina (CIBER-BBN), Zaragoza, Spain

E. Kuhl (✉)
Departments of Mechanical Engineering, Bioengineering, and Cardiothoracic Surgery, Stanford University, Stanford, CA 94305, USA
e-mail: ekuhl@stanford.edu

1 Motivation

Hypertension is characterized through a substantial elevation in blood pressure, which initiates the adaptation of vascular tissue. The immediate change, on a short-term scale, is the adaptation of smooth muscle cell contractile forces in the connective tissue, which can reduce the lumen diameter to compensate for the extra stresses. In addition, we can observe two long-term adaptation processes. The first long-term change is related to the secretion of collagen in the extracellular matrix, which gradually stiffens the arterial tissue. The second long-term change consists of the increase of smooth muscle cells both in volume and in number. Experimentally, this adaptation manifests itself in a thickening of the vessel wall. In this work, we focus on this latter phenomenon, the growth of smooth muscle cells in response to chronic hypertension.

Smooth muscle cells are responsible for vascular contraction, also known as myogenic tone [6,62], which is directly related to the intracellular calcium concentration and to the ion channels of the cell [9]. Vascular contraction attempts to compensate the over-stress in the vessel wall to maintain the same vessel diameter [27,51].

Smooth muscle cells typically grow through hypertrophy, by increasing their volume, through hyperplasia, by increasing their number, or through a combination of both [52,54]. This micro-structural change leads to the well-documented thickening of the vessel wall to restore the homeostatic stress state illustrated in Fig. 1. These changes are most pronounced in small or resistance vessels [15,49]. A multitude of experimental findings is related to hypertension-induced thickening of the arterial wall; many of them are related to drug performance, to the genetic expression of substances, and to the plain case of thickening. Some of these studies look at essential hypertension, while other assess hypertension

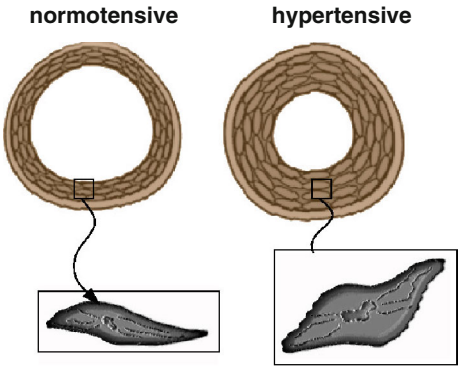

Fig. 1 Hypertensive anisotropic arterial growth. In contrast to the normtensive artery, *left*, the hypertensive artery, *right*, displays progressive smooth muscle cell growth resulting in chronic arterial wall thickening

by means of hypoxic states or ligands of some particular arteries.

Wiener et al. [68] studied aortas of hypertensive rats and observed a decrease in lumen diameter of 9 % and a thickness increase of 18 % from 182.5 μm in the normotensive state to 215.5 μm in hypertension. Owens and Schwartz [54] reported an increase of 35 % in smooth muscle cell size due to hyperplasia in the hypertensive rat aorta. The same authors showed an increase of 32.2 % in aortic mass and of 39.7 % in smooth muscle cell mass in Goldblatt hypertensive Sprague-Dawley rats [53]. Schofield et al. [61] studied the evolution of small human arteries and observed that the internal diameter decreased from 140 to 118 μm, while the thickness increased by 46.39 %. Since smaller arteries display a more pronounced contractile response, such a pronounced decrease could be caused by contractile phenomena. In fact, the above studies also addressed changes in the miogenic response in response to hypertension.

Studies on the carotid artery are also numerous. Boutouyrie et al. [5] reported a rise of the internal diameter in human carotids from 5.25 to 5.66 mm and an increase in thickness of 27.27 % from 0.487 to 0.572 mm. However, the same work showed a slight decrease in the lumen diameter from 2.33 to 2.32 mm in the radial artery accompanied by a 21.98 % increase in thickness. Fridez et al. [16] studied the influence of hypertension in carotid arteries of rats. They showed that the internal radius increased in hypertensive rats but it increased at a slower rate than in the control group. While the overall thickness increased by 58.4 % from 142 to 225 μm, this represented just a 30 % increase with respect to control group. The same group also observed that the thickness of the outer lamellar units grew more rapidly than that of the inner units. Eberth et al. [10] studied morphological changes in rat carotid arteries for a period of 56 weeks and found an increase in the internal radius from 531 to 592 μm, accompanied by an increase in thickness from 23.1 to 85.7 μm.

These results demonstrate how vascular adaptation can differ, not only between different arteries and species, but also within the same artery of the same species. Interspecimen variation, different levels of smooth muscle cell activation, genetic disorders, age, life style, and many more factors can cause this variability. To point out a last example, Feihl et al. [12] collected data from different authors who all studied small subcutaneous human arteries. While there was a strong quantitative variability in the degree of the adaptive response, the qualitative trends were all similar to the trends described above.

The computational study of growth has gained increasing attention in the theoretical and computational mechanics community, [1,33,48,65]. Mechanical modeling of growth has been addressed in different ways. Typically, growing biological tissues are considered as open systems [40]. Their different configurational settings and their numerical treatment within the finite element method are discussed in Kuhl and Steinmann [39]. Typically, we can distinguish two fundamental forms of growth: volume growth [28] and density growth [38]. The first allows for changes in volume while keeping the density constant, whereas the second maintains a constant volume while the density is allowed to change [41,46,47]. The works of Skalak et al. [63] and Rodriguez et al. [57] pioneered the underlying kinematic theory of volumetric growth. Within the past decade, various authors and groups have adopted and refined this kinematic concept [18,26,35].

An alternative approach towards growth is based on the constrained mixture theory [67], where several constituents of a tissue are allowed to growth independently [31,32]. A similar approach [22,23,37] was recently extended to reactive mixtures [2]. First attempts are now underway to correlate cardiovascular growth and remodeling to dynamic alterations in pressure and flow [8] and to fluid structure interaction phenomena [13,34]. We would also like to point out the early work of Fung and Liu [17], which showed that growth induces a change in the natural configuration associated with the notion of residual stress [56].

The objective of this work is to introduce a computational model for smooth muscle cell growth and embed it into the anisotropic microstructure of vascular tissue. We focus on smooth muscle cell growth in response to chronic hypertension and explore its impact on arterial wall thickening. First, we briefly reiterate the general mechanical background of soft tissue and growth mechanics. Next, we introduce smooth muscle cell growth as a stress- or strain-driven process, activated by an elevated pressure or stretch. We update the history of growth using an incremental, interative Newton–Raphson scheme. To calibrate our model by means of experimental data, we first simulate hypertensive smooth muscle cell growth in an idealized circular arterial cross section. To demonstrate the regional variation of growth, we then simulate growth in a human carotid artery reconstructed from

clinical images. We close by discussing the main results and the possible impact of our work.

2 Baseline elasticity of cardiovascular tissue

Two important aspects enter the mechanical characterization of cardiovascular tissue, the kinematically non-linear behavior and constitutively non-linear behavior of quasi-incompressible materials. We will briefly summarize both in the following subsections.

2.1 Kinematics of quasi-incompressiblity

First, we reiterate the basic equations of the kinematically non-linear behavior. Our most important kinematic quantity is the deformation gradient $\mathbf{F}$, the tangent of the nonlinear deformation map φ,

$$\mathbf{F} = \nabla_{\mathbf{X}} \varphi, \tag{1}$$

where the symbol $\nabla_{\mathbf{X}}$ denotes the spatial gradient with respect to the referential coordinates $\mathbf{X}$. We can then introduce the Jacobian $\mathrm{J} = \det(\mathbf{F})$ and the right Cauchy Green deformation tensor,

$$\mathbf{C} = \mathbf{F}^{\mathrm{t}} \cdot \mathbf{F}. \tag{2}$$

To account for the characteristic quasi-incompressibile behavior of soft biological tissues, we adopt a volumetric–isochoric decomposition of the deformation gradient [14,20],

$$\mathbf{F} = \mathrm{J}^{1/3} \bar{\mathbf{F}}. \tag{3}$$

The overbar is associated with the prefix isochoric and denotes the volume-preserving part. Accordingly, $\bar{\mathbf{F}}$ denotes the isochoric deformation gradient with $\det(\bar{\mathbf{F}}) = 1$, and

$$\bar{\mathbf{C}} = \bar{\mathbf{F}}^{\mathrm{t}} \cdot \bar{\mathbf{F}} \tag{4}$$

denotes the associated isochoric right Cauchy Green deformation tensor. It is convenient to introduce the first and fourth invariants,

$$\bar{I}_1 = \bar{\mathbf{C}} : \mathbf{I} \quad \text{and} \quad \bar{I}_4 = \bar{\mathbf{C}} : \mathbf{N} \tag{5}$$

where $\mathbf{N} = \mathbf{n} \otimes \mathbf{n}$ denotes the structural tensor defined in terms of the characteristic microstructural direction $\mathbf{n}$.

2.2 Constitutive equations of quasi-incompressibility

Second, we summarize the basic equations of the constitutively non-linear behavior. For soft biological tissues it is common to adapt the framework of hyperlasticity, based on the definition of a strain energy density function Ψ. To account for quasi-incompressiblity, we additively decompose this strain energy density function into volumetric and isochoric parts,

$$\Psi = \Psi_{\mathrm{vol}}(\mathrm{J}) + \Psi_{\mathrm{iso}}(\bar{\mathbf{C}}). \tag{6}$$

The volumetric contribution Ψ_{vol}, is primarily related to the water content in the tissue. The isochoric contribution Ψ_{iso}, is typically further split into an isotropic contribution related to the elastin content Ψ_{ela} and an anisotropic contribution related to the collagen fibers Ψ_{col}. From the evaluation of the dissipation inequality [29,45], we obtain the second Piola–Kirchhoff stress,

$$\mathbf{S} = 2\partial_{\mathbf{C}} \Psi = \mathbf{S}_{\mathrm{vol}} + \mathbf{S}_{\mathrm{iso}} \tag{7}$$

which consists of a volumetric part,

$$\mathbf{S}_{\mathrm{vol}} = 2\partial_{\mathbf{C}} \Psi_{\mathrm{vol}} = \mathrm{J}\, \partial_{\mathrm{J}} \Psi_{\mathrm{vol}}\, \mathbf{C}^{-1}, \tag{8}$$

and an isotropic part,

$$\mathbf{S}_{\mathrm{iso}} = 2\partial_{\mathbf{C}} \Psi_{\mathrm{iso}} = 2\partial_{\bar{\mathbf{C}}} \Psi_{\mathrm{iso}} : \partial_{\mathbf{C}} \bar{\mathbf{C}} = \mathrm{J}^{-2/3} \mathbb{P} : \bar{\mathbf{S}}. \tag{9}$$

Here $\bar{\mathbf{S}} = 2\,\partial_{\bar{\mathbf{C}}} \Psi_{\mathrm{iso}}$ is the fictitious second Piola–Kirchhoff stress and $\mathbb{P} = \mathbb{I} - \frac{1}{3}\,\mathbf{C}^{-1} \otimes \mathbf{C}$ denotes the fourth order projection tensor. Through the contravariant push forward operation, we obtain the Cauchy stress $\boldsymbol{\sigma}$,

$$\boldsymbol{\sigma} = \frac{1}{\mathrm{J}}\, \mathbf{F} \cdot \mathbf{S} \cdot \mathbf{F}^{\mathrm{t}}, \tag{10}$$

which is typically required for the finite element implementation. The tensor of tangent moduli, a fourth order tensor that relates incremental stresses and strains, is essential for a consistent finite element implementation. It represents the total derivative of the stress $\mathbf{S}$ with respect to the deformation tensor $\mathbf{C}$,

$$\mathbf{C} = 2\mathrm{d}_{\mathbf{C}} \mathbf{S} = \mathbf{C}_{\mathrm{vol}} + \mathbf{C}_{\mathrm{iso}}, \tag{11}$$

and consists of a volumetric contribution,

$$\mathbf{C}_{\mathrm{vol}} = 2\mathrm{d}_{\mathbf{C}} \mathbf{S}_{\mathrm{vol}} = 2\,\mathrm{J}\,\tilde{p}\,\mathbf{C}^{-1} \otimes \mathbf{C}^{-1} - 2\,\mathrm{J}\,p\,\mathbb{I}_{\mathbf{C}^{-1}}, \tag{12}$$

and an isochoric contribution,

$$\mathbf{C}_{\mathrm{iso}} = 2\mathrm{d}_{\mathbf{C}} \mathbf{S}_{\mathrm{iso}} = \mathbb{P} : \overline{\mathbf{C}} : \mathbb{P}^{\mathrm{t}} + \frac{2}{3}\,\mathrm{J}^{-2/3}\,\mathrm{tr}(\mathbf{S}_{\mathrm{iso}})\,\tilde{\mathbb{P}} - \frac{2}{3}\,[\,\mathbf{C}^{-1} \otimes \bar{\mathbf{S}} + \bar{\mathbf{S}} \otimes \mathbf{C}^{-1}\,]. \tag{13}$$

Here p denotes the hydrostatic pressure with $\tilde{p} = p + \mathrm{J}\,\partial_{\mathrm{J}} p$, and $\overline{\mathbf{C}} = 4\,\mathrm{J}^{-4/3}\,\partial_{\bar{\mathbf{C}} \otimes \bar{\mathbf{C}}} \Psi_{\mathrm{iso}}$ are the fictitious elastic tangent moduli [21]. In addition, we have introduced the following abbreviations for the fourth order tensors $\tilde{\mathbb{P}} = \mathbb{I}_{\mathbf{C}^{-1}} - \frac{1}{3}\,\mathbf{C}^{-1} \otimes \mathbf{C}^{-1}$ and $\mathbb{I}_{\mathbf{C}^{-1}} = \frac{1}{2}[\mathbf{C}^{-1} \overline{\otimes} \mathbf{C}^{-1} + \mathbf{C}^{-1} \underline{\otimes} \mathbf{C}^{-1}]$, where the non-standard fourth order tensor products take the following interpretation, $\{\bullet \overline{\otimes} \circ\}_{ijkl} = \{\bullet\}_{ik}\,\{\circ\}_{jl}$ and $\{\bullet \underline{\otimes} \circ\}_{ijkl} = \{\bullet\}_{il}\,\{\circ\}_{jk}$.

Table 1 Elastic material parameters for media and adventitia of human carotid artery (CCA) and of human internal carotid artery (ICA) [60,64]

	μ (kPa)	k_1 (kPa)	k_2 (-)
CCA media	4.31	2.19	4.15
CCA adventitia	0.04	7.32	66.81
ICA media	11.01	2.14	20.72
ICA adventitia	0.04	15.97	51.01

Remark 1 (*Elasticity of arterial tissue*) The modeling of arterial tissue has been widely discussed in literature [30]. It is common to describe the isochoric response Ψ_{iso} by means of an isotropic contribution for elastin, Ψ_{ela}, and an anisotropic contribution for collagen, Ψ_{col},

$$\Psi_{\text{iso}}(\overline{I}_1, \overline{I}_4) = \Psi_{\text{ela}}(\overline{I}_1) + \Psi_{\text{col}}(\overline{I}_4)\,,$$

where $\overline{I}_1$ and $\overline{I}_4$ are the first and fourth invariant of the isochoric part of the deformation according to Eq. (5). The isotropic elastin part is typically parameterized in terms of a single stiffness parameter μ, e.g., as

$$\Psi_{\text{ela}}(\overline{I}_1) = \mu\,[\,\overline{I}_1 - 3\,]\,.$$

The anisotropic collagen part has been discussed intensely in the literature. O'Connell et al. [50] have studied the structural organization of the arterial layers, and found that the collagen fibers follow a helicoidal distribution from the outer to the inner layer. Collagen fibers are bundled around smooth muscle cells and around some secondary fibrils, which cross-link the main collagen fibers. In the adventitia, the outermost layer of the artery, collagen displays a rather random orientation. In the media, the middle layer, collagen and smooth muscle cells form organized sublayers with slightly varying preferred orientations. Garcia [19] reported an almost circumferential orientation of the collagen fibers in the media of carotid arteries. Here, for simplicity, we adopt the following ansatz for the collagen part of the free energy [21],

$$\Psi_{\text{col}}(\overline{I}_1) = \frac{k_1}{2k_2}[\,\exp(k_2[\overline{I}_1 - 1]^2) - 1\,]\,.$$

Based on experimental data [64], we identify the mechanical parameters μ, k_1, and k_2 in different regions of the human carotid artery. Table 1 summarizes the identified material parameter values. Figure 2 illustrates the regional variation of the mechanical parameters along the carotid artery.

3 Growth of cardiovascular tissue

3.1 Kinematics of growth

Within the framework of finite growth, the key kinematic assumption is the multiplicative decomposition of the deformation gradient $\mathbf{F}$ into an elastic part $\mathbf{F}_{\text{e}}$ and a growth part $\mathbf{F}_{\text{g}}$ [57],

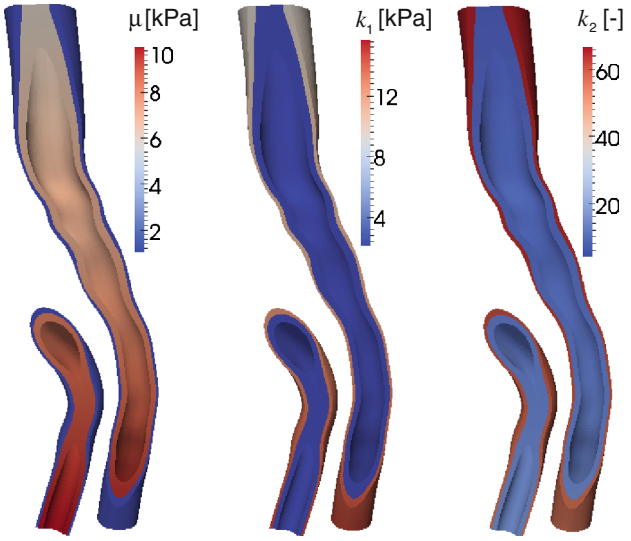

Fig. 2 Regional variation of material parameters μ, k_1, and k_2 along human carotid artery

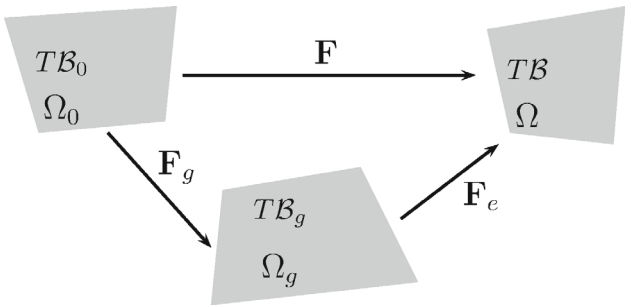

Fig. 3 Kinematics of finite growth. Multiplicative decomposition of the deformation gradient $\mathbf{F}$ into an elastic tensor $\mathbf{F}_{\text{e}}$ and a growth tensor $\mathbf{F}_{\text{g}}$

$$\mathbf{F} = \mathbf{F}_{\text{e}} \cdot \mathbf{F}_{\text{g}}\,. \tag{14}$$

The underlying concept is adopted from the multiplicative decomposition in finite plasticity [43] and illustrated in Fig. 3. While we can think of the growth tensor $\mathbf{F}_{\text{g}}$ as a second-order variable to characterize arbitrary forms of isotropic or anisotropic growth, here we will parameterize the growth tensor exclusively in terms of a single scalar-valued variable, the growth multiplier ϑ [24]. This approach is conceptually generic and can be easily adapted to model volume growth [28], area growth [7], and fiber growth [70]. We denote the Jacobians of the elastic tensor and of the growth tensor as $\text{J}_{\text{e}} = \det(\mathbf{F}_{\text{e}})$ and $\text{J}_{\text{g}} = \det(\mathbf{F}_{\text{g}})$, such that

$$\text{J} = \text{J}_{\text{e}}\,\text{J}_{\text{g}}\,. \tag{15}$$

We can then introduce the elastic right Cauchy Green tensor,

$$\mathbf{C}_{\text{e}} = \mathbf{F}_{\text{e}}^{\text{t}} \cdot \mathbf{F}_{\text{e}} = \mathbf{F}_{\text{g}}^{-\text{t}} \cdot \mathbf{C} \cdot \mathbf{F}_{\text{g}}^{-1}\,, \tag{16}$$

and relate it to the total right Cauchy Green tensor $\mathbf{C}$ using the inverse growth tensor.

Remark 2 (*Growth of arterial tissue*) Motivated by experimental observations of smooth muscle cell growth [52–54], we specify the growth tensor as

$$\mathbf{F}_{\mathrm{g}} = \mathbf{I} + [\,\vartheta - 1\,]\,\mathbf{n}\otimes\mathbf{n}\,,$$

where ϑ is the scalar-valued growth multiplier that characterizes the amount of growth and $\mathbf{n}$ is a characteristic structural direction [25]. The sensitivity of growth with respect to the growth multiplier then takes the following simple form,

$$\partial_{\vartheta}\mathbf{F}_{\mathrm{g}} = \mathbf{n}\otimes\mathbf{n}\,,$$

If we choose $\mathbf{n}$ to be alined with the radial direction, this particular format of the growth tensor characterizes smooth muscle cell thickening in the radial direction while the cells length remains constant. This type of growth is conceptually similar to hypertrophic growth in the heart [55].

3.2 Constitutive equations of growth

Next, we embed the kinematic characterization of growth into the hyperelastic baseline description introduced in Sect. 2.2. To this end, we reparameterize the free energy function $\Psi(\mathbf{C}_{\mathrm{e}})$, which was initially parameterized in terms of the elastic deformation tensor $\mathbf{C}_{\mathrm{e}}$, in terms of the total deformation tensor $\mathbf{C}$ and the growth tensor $\mathbf{F}_{\mathrm{g}}$, such that $\Psi(\mathbf{C},\mathbf{F}_{\mathrm{g}})$ and

$$\dot{\Psi} = \partial_{\mathbf{C}}\Psi : \dot{\mathbf{C}} + \partial_{\mathbf{F}_{\mathrm{g}}}\Psi : \dot{\mathbf{F}}_{\mathrm{g}}\,. \tag{17}$$

Thermodynamic considerations motivate the introduction of the second Piola–Kirchhoff stress,

$$\mathbf{S} = 2\partial_{\mathbf{C}}\Psi = 2\partial_{\mathbf{C}_{\mathrm{e}}}\Psi : \partial_{\mathbf{C}}\mathbf{C}_{\mathrm{e}} = \mathbf{F}_{\mathrm{g}}^{-1}\cdot\mathbf{S}_{\mathrm{e}}\cdot\mathbf{F}_{\mathrm{g}}^{-\mathrm{t}}\,. \tag{18}$$

Here, $\mathbf{S}_{\mathrm{e}} = 2\,\partial_{\mathbf{C}_{\mathrm{e}}}\Psi$ is the classic elastic second Piola–Kirchhoff stress as introduced in Eq. (7). To derive the Lagrangian tangent moduli, essential for a consistent finite element implementation, we evaluate the total derivative of the second Piola–Kirchhoff stress $\mathbf{S}$ with respect to the right Cauchy Green deformation tensor $\mathbf{C}$,

$$\begin{aligned}\mathbf{C} = 2\mathrm{d}_{\mathbf{C}}\mathbf{S} &= \mathbf{C}_{\mathrm{e}} + \mathbf{C}_{\mathrm{g}}\\ &= 2\partial_{\mathbf{C}}\mathbf{S}\big|_{\mathbf{F}_{\mathrm{g}}} + 2\partial_{\mathbf{C}}\mathbf{S}\big|_{\mathbf{F}}\\ &= 2\partial_{\mathbf{C}}\mathbf{S}\big|_{\mathbf{F}_{\mathrm{g}}} + 2\left[\partial_{\mathbf{F}_{\mathrm{g}}}\mathbf{S} : \partial_{\vartheta}\mathbf{F}_{\mathrm{g}}\right]\otimes\partial_{\mathbf{C}}\vartheta\big|_{\mathbf{F}}.\end{aligned} \tag{19}$$

The first term of Eq. (19) represents the pull back of the elastic tangent moduli to the undeformed reference configuration,

$$\mathbf{C}_{\mathrm{e}} = 2\mathrm{d}_{\mathbf{C}}\mathbf{S}\big|_{\mathbf{F}_{\mathrm{g}}} = [\mathbf{F}_{\mathrm{g}}^{-1}\overline{\otimes}\mathbf{F}_{\mathrm{g}}^{-1}] : 2\mathrm{d}_{\mathbf{C}_{\mathrm{e}}}\mathbf{S}_{\mathrm{e}} : [\mathbf{F}_{\mathrm{g}}^{-\mathrm{t}}\overline{\otimes}\mathbf{F}_{\mathrm{g}}^{-\mathrm{t}}]\,. \tag{20}$$

Here, $2\mathrm{d}_{\mathbf{C}_{\mathrm{e}}}\mathbf{S}_{\mathrm{e}}$ are the classic elastic tangent moduli as introduced in Eq. (11). The second term of Eq. (19) is related to the linearization of the growth model,

$$\mathbf{C}_{\mathrm{g}} = 2\mathrm{d}_{\mathbf{C}}\mathbf{S}\big|_{\mathbf{F}} = 2\left[\partial_{\mathbf{F}_{\mathrm{g}}}\mathbf{S} : \partial_{\vartheta}\mathbf{F}_{\mathrm{g}}\right]\otimes\partial_{\mathbf{C}}\vartheta\big|_{\mathbf{F}}\,. \tag{21}$$

The first term, $\partial_{\mathbf{F}_{\mathrm{g}}}\mathbf{S}$, is conceptually generic,

$$\begin{aligned}\partial_{\mathbf{F}_{\mathrm{g}}}\mathbf{S} = &-[\,\mathbf{F}_{\mathrm{g}}^{-1}\overline{\otimes}\mathbf{S} + \mathbf{S}\underline{\otimes}\mathbf{F}_{\mathrm{g}}^{-1}\,]\\ &-[\,\mathbf{F}_{\mathrm{g}}^{-1}\overline{\otimes}\mathbf{F}_{\mathrm{g}}^{-1}\,] : \frac{1}{2}\,\mathbf{C} : [\,\mathbf{F}_{\mathrm{g}}^{-\mathrm{t}}\overline{\otimes}\mathbf{C}_{\mathrm{e}} + \mathbf{C}_{\mathrm{e}}\underline{\otimes}\mathbf{F}_{\mathrm{g}}^{-\mathrm{t}}].\end{aligned} \tag{22}$$

The second term, $\partial_{\vartheta}\mathbf{F}_{\mathrm{g}}$, is specific to the format of the growth tensor $\mathbf{F}_{\mathrm{g}}$ as discussed in Remark 2, i.e., in our case $\partial_{\vartheta}\mathbf{F}_{\mathrm{g}} = \mathbf{n}\otimes\mathbf{n}$. The third term, $\partial_{\mathbf{C}}\vartheta$, is specific to the evolution of growth ϑ, which we will specify in Remarks 3 and 4 for the stress- and strain-driven case. To obtain the Eulerian tangent moduli $\mathbf{c}$ for the finite element implementation, we push Lagrangian tangent moduli $\mathbf{C}$ of Eq. (19) forward to the deformed configuration,

$$\mathbf{c} = \frac{1}{\mathrm{J}}\,[\,\mathbf{F}\overline{\otimes}\mathbf{F}\,] : \mathbf{C} : [\,\mathbf{F}^{\mathrm{t}}\overline{\otimes}\mathbf{F}^{\mathrm{t}}\,]\,. \tag{23}$$

Last, we define the evolution of the growth multiplier [24],

$$\dot{\vartheta} = k(\vartheta)\,\phi(\boldsymbol{\Xi})\,. \tag{24}$$

Here $\boldsymbol{\Xi}$ represents driving force for growth and k is a limiting function that ensures that the tissue does not grow unboundedly [44],

$$k = \frac{1}{\tau}\left[\frac{\vartheta^{\max} - \vartheta}{\vartheta^{\max} - 1}\right]^{\gamma} \tag{25}$$

with $\partial_{\vartheta}k = -\gamma\,k/[\vartheta^{\max} - \vartheta]$. Growth evolves in time according to three parameters, the maximum amount of growth $\vartheta^{\max}$, the adaptation speed τ, and the non-linearity of the growth process γ [28]. The function $\phi(\boldsymbol{\Xi})$ represents the growth criterion similar to the flow rule in the theory of plasticity. In the following, we discuss two different mechanisms to drive the evolution of growth, stress and strain.

3.3 Numerical implementation

For the numerical implementation, we integrate the evolution of growth in time using an implicit Euler backward scheme,

$$\dot{\vartheta} = [\vartheta^{\mathrm{n}+1} - \vartheta^{\mathrm{n}}]/\Delta t\,, \tag{26}$$

where Δt denotes the current time increment. This allows us to introduce the discrete local residual,

$$\mathcal{R} = \vartheta^{\mathrm{n}+1} - \vartheta^{\mathrm{n}} - k(\vartheta)\phi(\boldsymbol{\Xi})\Delta t\,. \tag{27}$$

To solve this non-linear equation, we expand the residual up to the first order term. We can then solve this equation, $\mathcal{R} + \partial_{\vartheta}\mathcal{R}\,\Delta\vartheta \doteq 0$, within an iterative Newton–Raphson scheme. With the tangent of the residual,

$$\mathcal{K} = \partial_{\vartheta}\mathcal{R} = 1 - [\,k\,\partial_{\vartheta}\phi + \partial_{\vartheta}k\,\phi\,]\,\Delta t\,, \tag{28}$$

we can incrementally update the growth multiplier $\vartheta^{\mathrm{n}+1} \leftarrow \vartheta^{\mathrm{n}} - \mathcal{R}/\mathcal{K}$ until the residual $\mathcal{R}$ has converged towards a small enough user-defined tolerance. Table 2 summarizes the local algorithmic treatment of the numerical procedure, which can

Table 2 Algorithm for implicit Euler scheme of stress- or strain-driven growth

Input: $\mathbf{F}^{t+1}, \vartheta^t$

1. Evaluate kinematics $\mathbf{C}^{t+1}, \mathbf{F}_e^{t+1} = \mathbf{F}^{t+1} \cdot \mathbf{F}_g^t$ and stresses $\mathbf{S}_e^{t+1}, \mathbf{S}^{t+1}$
2. Check for growth
   IF $(\lambda_{smc} > \lambda_{crit})$
   THEN Determine new growth multiplier
   WHILE $\mathcal{R} >$ tol DO
   Calculate residual $\mathcal{R} = \vartheta^{n+1} - \vartheta^n - k(\vartheta)\phi(\boldsymbol{\Xi})\Delta t$
   Calculate tangent $\mathcal{K} = 1 - [\, k\, \partial_\vartheta \phi + \partial_\vartheta k\, \phi\,]\, \Delta t$
   Update growth $\vartheta^{n+1} \leftarrow \vartheta^n - \mathcal{R}/\mathcal{K}$
   END
3. Compute Cauchy stresses $\boldsymbol{\sigma}^{t+1}$
   Compute tangent moduli $\mathbf{c}^{t+1}$

Output: $\boldsymbol{\sigma}^{t+1}, \mathbf{c}^{t+1}, \vartheta^{n+1}$

be easily embedded into any finite element setting at the constitutive level.

Remark 3 (*Stress-driven growth*) Stress is the most popular driving force for growth, in particular in the biomedical and clinical communities, and it is widely used for growth within the cardiovascular system [24]. Accordingly, we can introduce the evolution of the growth multiplier,

$$\dot{\vartheta} = k(\vartheta)\phi(\mathbf{M}_e)\,,$$

using a stress-driven growth criterion [24,36],

$$\phi(\mathbf{M}_e) = p_e - p_{crit} \quad \text{with} \quad p_e = \text{tr}(\mathbf{M}_e)\,.$$

Here, $\mathbf{M}_e = \mathbf{C}_e \cdot \mathbf{S}_e$ is the elastic Mandel stress, its trace, $p_e = \text{tr}(\mathbf{M}_e)$, is a measure of the pressure in the arterial wall, and p_{crit} denotes the physiological pressure above which growth occurs. The derivative of the growth criterion with respect to the growth multiplier ϑ required for the consistent linearization in Eq. (28) then reads

$$\partial_\vartheta \phi = -\partial_\vartheta \mathbf{C}_e : \mathbf{S}_e + \mathbf{C}_e : \partial_\vartheta \mathbf{S}_e\,,$$

with $\partial_\vartheta \mathbf{C}_e = -\mathbf{F}_g^{-t} \cdot \partial_\vartheta \mathbf{F}_g^t \cdot \mathbf{C}_e - \mathbf{C}_e \cdot \partial_\vartheta \mathbf{F}_g \cdot \mathbf{F}_g^{-1}$ and $\partial_\vartheta \mathbf{S}_e = \frac{1}{2}\mathbf{C}_e : \partial_\vartheta \mathbf{C}_e$. Last, to complete the tangent moduli in (19), we provide the derivative of the growth multiplier with respect to the Cauchy–Green strain tensor,

$$\partial_{\mathbf{C}} \vartheta = \frac{k\,\Delta t}{\mathcal{K}} \left[\, \frac{1}{2}\, \mathbf{C}_e : \mathbf{C}_e + \mathbf{S}_e \,\right].$$

Within a finite element setting, stress-driven growth requires an additional internal iteration to update the growth multiplier, since its driving force, the current stress, is typically not known a priori.

Remark 4 (*Strain-driven anisotropic growth*) Strain is a popular driving force for growth, in particular in cell biology and mechanotransduction, since cells are equipped with various mechanisms to sense and respond to strains [72]. Adopting the concept of strain-driven growth, we can introduce the evolution of the growth multiplier,

$$\dot{\vartheta} = k(\vartheta)\phi(\mathbf{C}_e)\,,$$

using a strain-driven growth criterion [7,24],

$$\phi(\mathbf{C}_e) = \lambda_e - \lambda_{crit} \quad \text{with} \quad \lambda_e = [\, \mathbf{n} \cdot \mathbf{C}_e \cdot \mathbf{n}\,]^{1/2}\,.$$

Here λ_{crit} denotes a physiological stretch above which growth occurs and $\mathbf{n}$ is a characteristic microstructural direction. If we assume that our smooth muscle cells and collagen fibers are collectively aligned along this direction $\mathbf{n}$, and that they undergo an affine deformation, they sense the same elastic stretches, $\lambda_e = \lambda_{smc} = \lambda_{col}$, which act as driving force for growth. The remaining term for the local tangent in Eq. (28) then simply reads

$$\partial_\vartheta \phi = -\lambda/\lambda_g^2\,,$$

and the global tangent term in Eq. (19) becomes

$$\partial_{\mathbf{C}} \vartheta = \frac{k\,\Delta t}{\mathcal{K}} \left[\, \frac{1}{2\,\lambda}\, \mathbf{n} \otimes \mathbf{n} \right],$$

where $\lambda = [\, \mathbf{n} \cdot \mathbf{C} \cdot \mathbf{n}\,]^{1/2}$ is the total stretch along the mircostructural direction $\mathbf{n}$. Unlike stress-driven growth, strain-driven growth does not require an additional internal iteration to update the growth multiplier, since its driving force, the current strain, is typically known a priori. Strain-driven growth is therefore computationally more stable and robust.

4 Arterial growth in hypertension

In this section, we illustrate the characteristic features of the proposed growth model by means of two examples. First, to compare stress and strain driven growth, we simulate hypertensive growth in a circular cross section of an artery. Second, to illustrate the regional variation of growth, we simulate hypertensive strain-driven growth in a human carotid artery. Table 1 summarizes the three elastic material parameters, the elastic stiffness μ, the collagen stiffness k_1, and the nonlinearity of the collagen contribution k_2 for both the media and the adventitia. Table 3 summarizes the three growth parameters, the maximum amount of growth ϑ^{max}, the adaptation speed τ, and the non-linearity of the growth process γ for both examples. To initiate growth, we adopt the following simulation protocol:

Table 3 Growth material parameters for circular cross section of an artery in Sect. 4.1 and for human carotid artery in Sect. 4.2 [16]

	ϑ^{max} (-)	τ (1/days)	γ (-)
4.1 Circular cross section	2.0	1.0	2.0
4.2 Human carotid artery	1.6	10.0	3.0

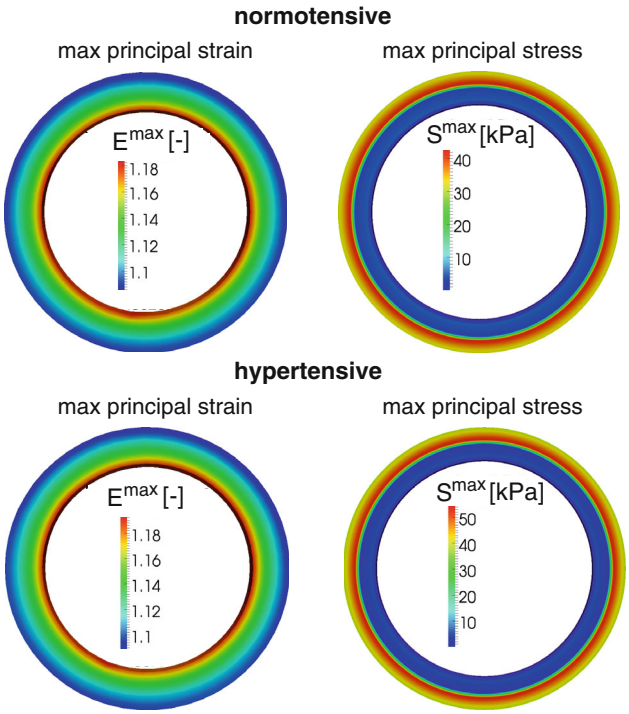

Fig. 4 Normotensive and hypotensive conditions in a cylindrical prototype artery with maximum principal strains, *left*, and stresses, *right*

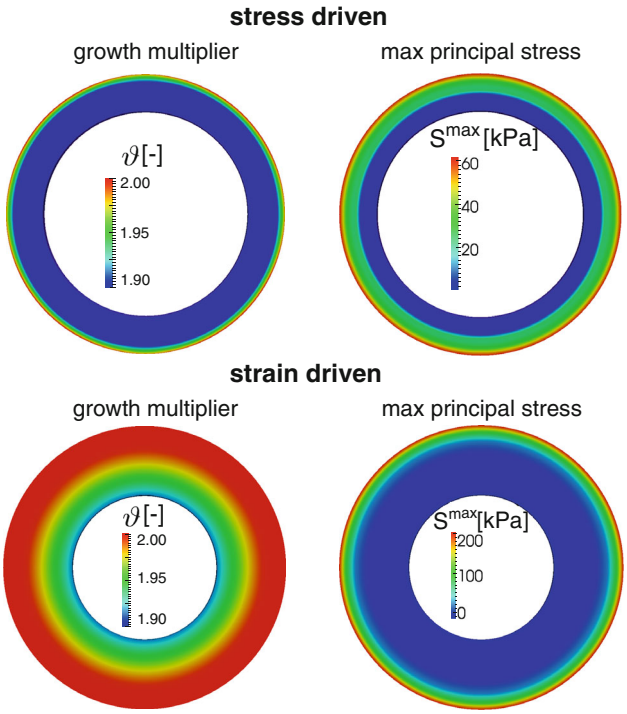

Fig. 5 Stress driven, *top*, and strain driven, *bottom*, growth in a cylindrical prototype artery with growth multiplier, *left*, and maximum principal stresses, *right*

1. Gradually pressurize an artery up to the normotensive state at a physiological pressure level of 13.3 kPa.
2. Calculate the resulting profiles of the critical physiological stretch λ_{crit} and pressure p_{crit} and store their values locally in a pointwise fashion.
3. Gradually increase the pressure up to the hypertensive state at a chronically elevated pressure level of 16.0 kPa.
4. Allow the tissue to grow chronically to compensate for the extra deformation and stress.

Existing models typically treat the critical physiological stretch λ_{crit} and pressure p_{crit} as constant homogeneous material parameters, which do not vary in space. Here we associate these critical values with the normotensive state. As such, these threshold values for growth are naturally associated with the physiological pressure and inherently display transmural and axial longitudinal variations across the arterial wall.

4.1 Growth in a cylindrical cross section of an artery

In the first example, we simulate hypertensive growth in a circular cross section of the arterial wall. In particular, we seek to answer the question, which driving force is more suitable for hypertensive growth, stress or strain. We simulate an idealized circular arterial slice, discretized with separate medial and adventitial layers. We systematically compare stress-driven growth, $\phi(\mathbf{M}_e) = p(\mathbf{M}_e) - p_{\text{crit}}$ according to Remark 3, with strain-driven growth, $\phi(\mathbf{C}_e) = \lambda_e(\mathbf{C}_e) - \lambda_{\text{crit}}$ according to Remark 4.

Figures 4 and 5 illustrate a finite element simulation of growth in a cylindrical cross section of the arterial wall, displayed in the deformed current configuration. Figure 4 displays the maximum principal strains and stresses under normotensive and hypertensive conditions. Figure 5 compares the growth multiplier and the maximum principal stresses for strain- and stress-driven growth. The arterial wall thickness and the regional profiles of the growth multiplier differ substantially for the strain- and stress-driven cases.

For the stress-driven case, as displayed in Fig. 5, bottom row, growth increases radially from inward to outward. Since the adventitial layer is much stiffer than the medial layer, this results in higher stresses in the adventitia, making it grow much faster in the stress-driven case. Moreover, the higher growth rate in the adventitia initiates a marked perpendicular expansion towards the center thereby decreasing the circumferential dimension of the media. For the strain-driven case, growth also increases radially, but significantly smoother than for the stress-driven case. For the first time, in contrast to previous studies [28,58], we have simulated growth in an artery wall with distinct layers and distinct stiffnesses. Our results show that it is critical to account for the different properties in different layers to predict experimental findings. As we have discuss in the introduction, arterial thickening occurs mainly in the media, caused by hypertrophy and hyperplasia of the smooth mus-

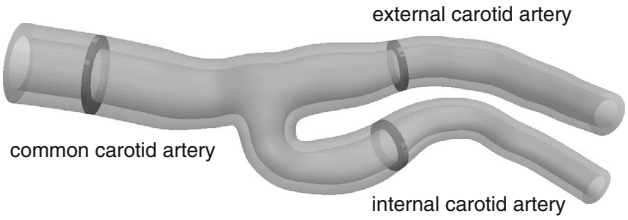

Fig. 6 Human carotid artery with three representative cross-sections in the common carotid artery, the internal carotid artery, and the external carotid artery, *highlighted in dark*

cle cells. For the stress-driven stimulus, growth seems to occur mainly in the adventitia, which would contradict these findings.

Strain-driven growth, as displayed in Fig. 5, top row, displays a more uniform growth distribution across the thickness. Since the circumferential stretch is more uniform than the stress distribution, growth occurs in a more distributed way, which seems to favorably agree with experimental findings.

The debate about the most adequate driving force for different processes in cells, e.g., cell differentiation or cell migration, remains vivid and still ongoing. Along these lines, the choice of a stress- or strain-driven approach to characterize hypertensive growth still remains unclear. From our results we conclude that growth in arterial tissue is highly sensitive to the choice of the underlying mechanical stimulus. In the particular case of growth in arteries it is known that growth occurs primarily in the media, since this is where the smooth muscle cells are situated. To better characterize the constitutive response of the arterial wall, we will from now on assume that smooth muscle cell growth is allowed to occur only in the medial layer. Moreover, we assume that the smooth muscle cell stretch is the mechanical variable that drives the growth process.

4.2 Growth in a human carotid artery

In the second example, we simulate hypertensive growth in a human carotid artery. In particular, we explore the regional distribution of growth across the bifurcated arterial segment. Figure 6 displays the geometry of the artery, which we discretize with 166,408 tri-linear brick elements. The discretization accounts for separate medial and adventitial layers. Following Remark 4, we adopt a strain-driven approach towards arterial growth based on the following growth criterion, $\phi(\mathbf{C}_e) = \lambda_e - \lambda_{crit}$. This implies that the smooth muscle cell stretch $\lambda_e = \lambda_{smc} = [\,\mathbf{n}\cdot\mathbf{C}_e\cdot\mathbf{n}\,]^{1/2}$ is the driving force for growth. To illustrate the features of the proposed approach, we compare our simulation with experimental findings [16]. We begin by studying the growth process in a representative slice of the common carotid artery as indicated in Fig. 6.

Figure 7, top, shows the evolution of a representative smooth muscle cell in the medial layer of the common carotid artery. The smooth muscle cell size increases in the radial direction while the longitudinal direction remains constant. Figure 7, bottom, shows the evolution of growth in a circular section of the deformed common carotid artery at different time steps. In response to hypertension, the maximum growth multiplier increases to $\vartheta = 1.47$, indicating an increase of smooth muscle cell thickness of almost 50 %.

Figure 8 shows the evolution of the growth multiplier over a period of 100 days, both for the experimental measurements in [16] and for the computational simulation with our model. Results displays a similar tendency throughout the

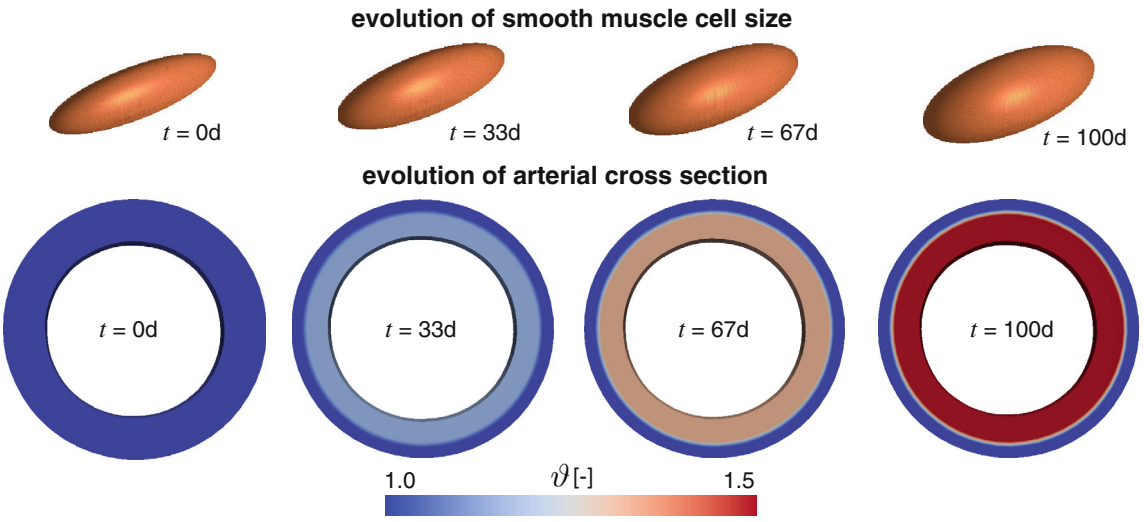

Fig. 7 Growth of a representative smooth muscle cell in the medial layer of the common carotid artery and its effect of the circular section at characteristic time steps. In response to hypertension, the growth multiplier gradually increases to $\vartheta = 1.47$, indicating an increase of smooth muscle cell thickness of almost 50 %

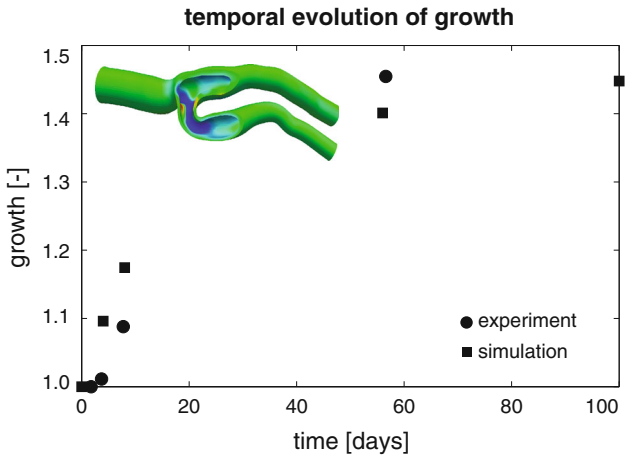

Fig. 8 Temporal evolution of growth in human carotid artery. *Circles* represent experimentally measured growth [16]; *squares* represent computationally simulated growth

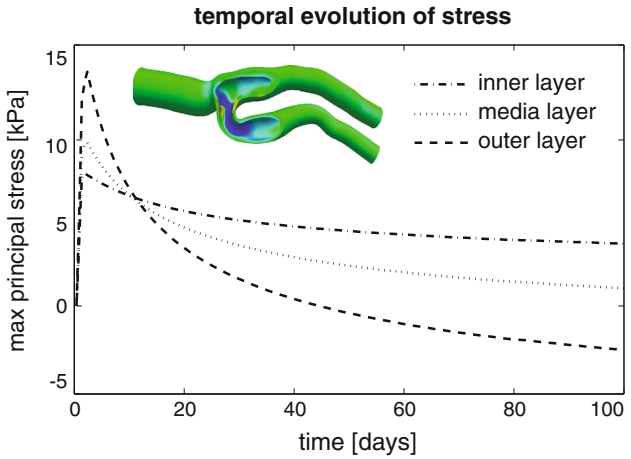

Fig. 9 Temporal evolution of maximum principal stresses in inner, medial, and outer layers of human carotid artery

growth process. Our results slightly overestimate the amount of growth during the first few days, and slightly underestimate the amount of growth long time.

Figure 9 displays the evolution of the maximum principal stresses in inner, medial, and outer layers of a human carotid artery. Stresses in the medial layer decrease as a result of smooth muscle cell growth. Smooth muscle cell growth, myogenic tone, and other physiological process have the common goal to reduce elevated wall stress caused by hypertension. Their ultimate goal is to bring the wall stress back to its physiological range, i.e., reduce its values towards the normotensive situation. As the growth multiplier ϑ increases, the growth tensor $\mathbf{F}_{\mathrm{g}}$ increases and causes the elastic tensor $\mathbf{F}_{\mathrm{e}}$ to decrease. This reduces the elastic stress $\mathbf{S}_{\mathrm{e}}$. While the media grows and its stresses decrease, stresses in the adventitia increase markedly. The stress increase in the adventitia is caused by the radial expansion of the media.

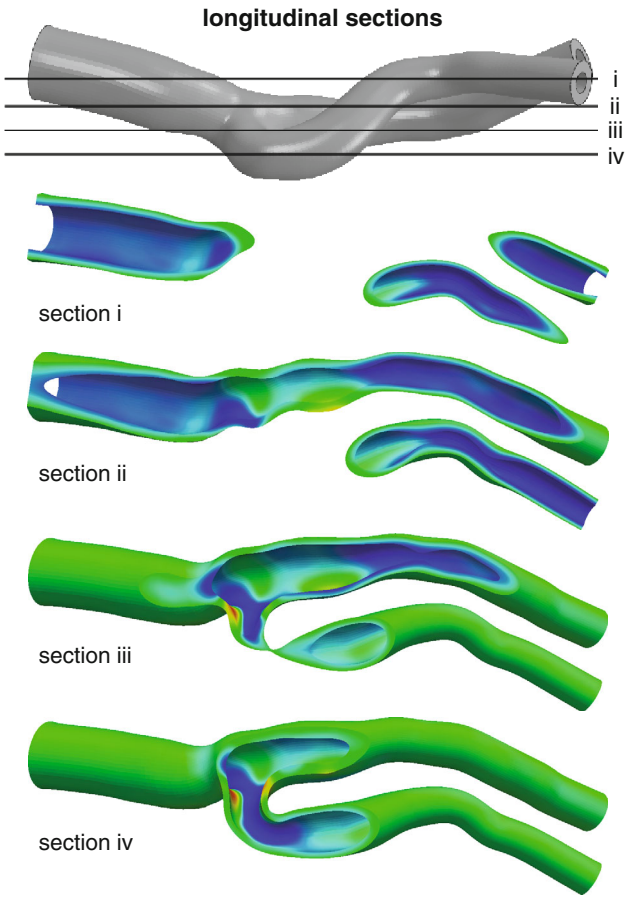

Fig. 10 Growth in different *longitudinal sections* of the human carotid artery at $t = 100$ days of hypertension

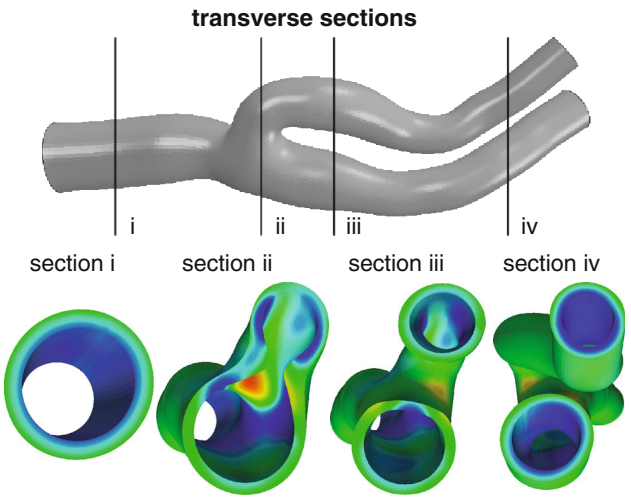

Fig. 11 Growth in different *transverse sections* of the human carotid artery at $t = 100$ days of hypertension

Figures 10 and 11 display growth in four representative longitudinal and transverse sections of the human carotid artery. The contour plots are displayed on the deformed current configuration after $t = 100$ days of hypertension. Simi-

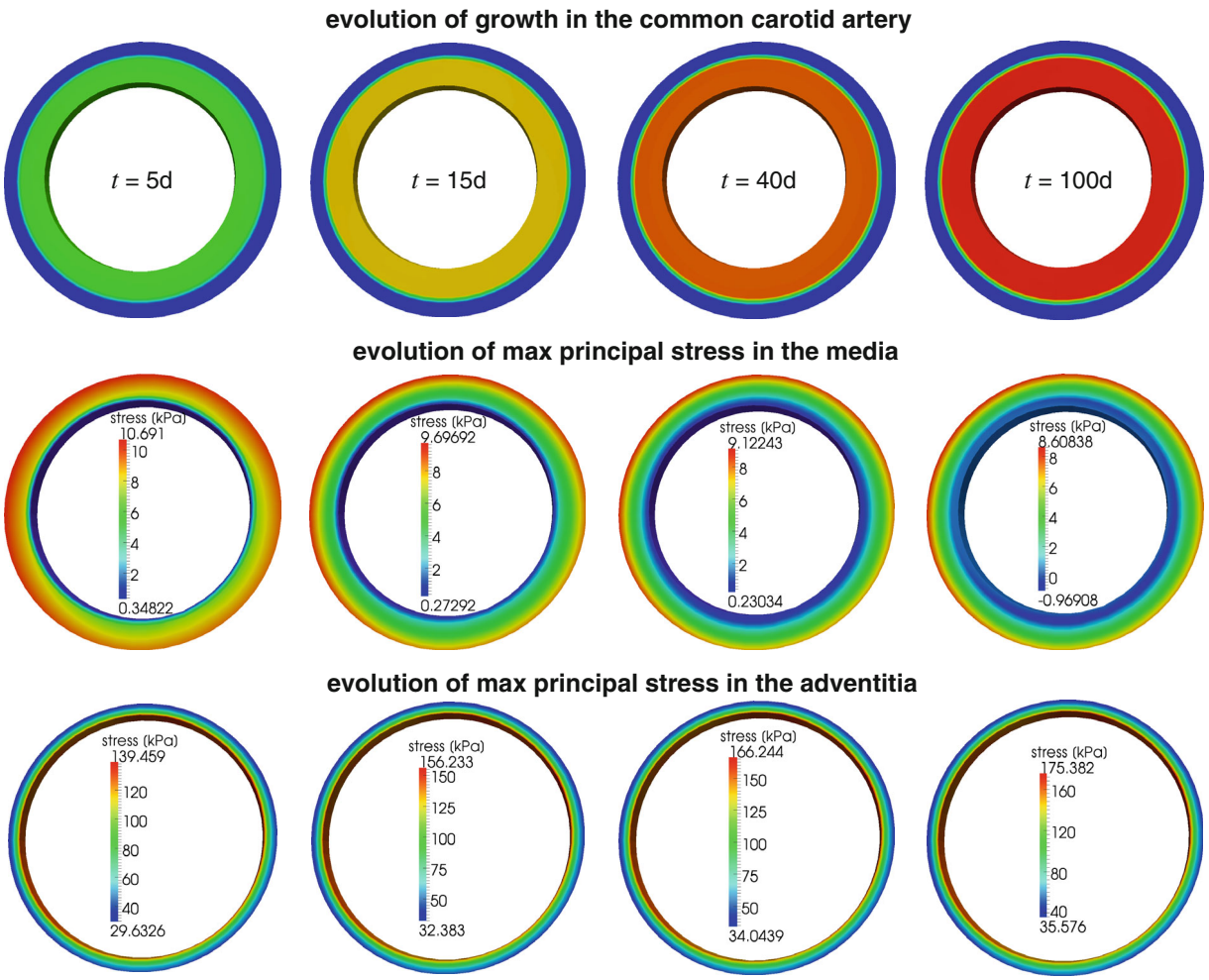

Fig. 12 Spatio-temporal evolution of growth in a representative slice of the common carotid artery. Growth multiplier, *top*, maximum principal stresses in the adventitia, middle, and maximum principal stresses in the media, *bottom* at 5, 15, 40, and 100 days of hypertension

lar to the findings in Sect. 4.1, growth is heterogeneous across the wall thickness, with smaller growth at the inner and larger growth at the outer layer. Growth also displays variations along the direction of flow.

Last, we summarize the spatio-temporal evolution of growth in three representative slices of the human carotid artery as highlighted in Fig. 6. Figures 12, 13, and 14 show the evolution of the growth multiplier and of the maximum principal stresses in the adventitia and media of the common, external, and internal carotid artery. The snap shots display the growth and stress contours on the deformed current configuration at different points in time. Growth and stress display similar trends in all three sections. This is in agreement with the smooth variations in stretch between the normotensive and the hypertensive states. Stresses in the adventitia increase by 20 %, while stresses in the media decrease by 25 % in the common carotid artery, by 13 % in the external carotid artery, and by 7 % in the internal carotid artery, respectively.

5 Discussion

Growth and remodeling of living systems has advanced to a rapidly growing field of research within the past decade [1]. Many recent studies focus on shedding light on different kinematic formulations, alternative balance equations, appropriate evolution equations, and suitable mechanical stimuli [48]. Here we have adapted the classical kinematic decomposition of the deformation gradient into an elastic and a growth part [43,57]. We have discussed microstructurally-motivated evolution equations for growth [25], and systematically compared different mechanical stimuli for the growth process [42]. To discretize the governing equations in time and space, we have applied an implicit Euler backward finite difference scheme in time and a geometrically nonlinear finite element scheme in space. To efficiently and robustly solve the set of governing equations, we have linearized the growth formulation consistently and embedded it into a local Newton iteration at the integration point level. The algorithm con-

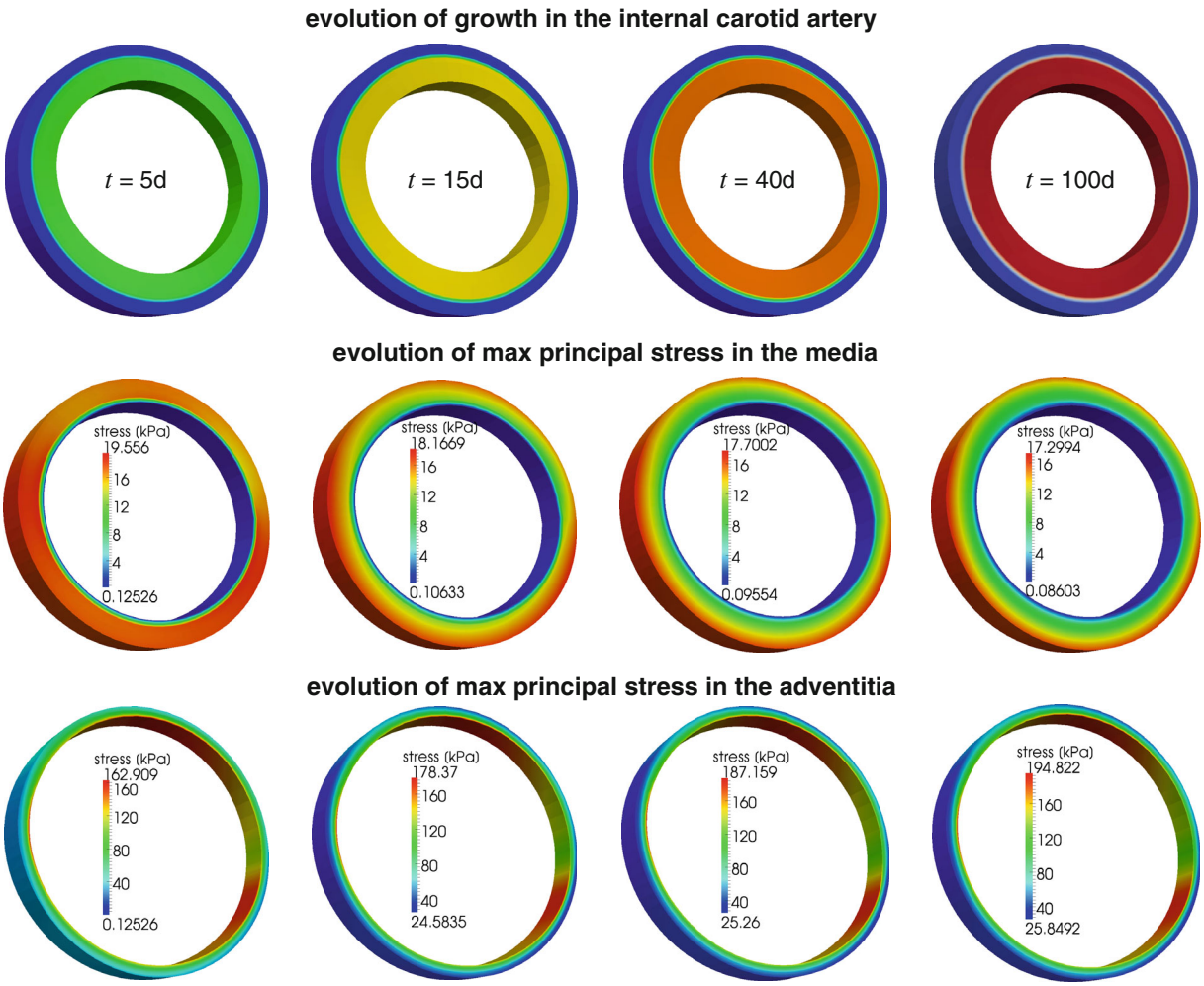

Fig. 13 Spatio-temporal evolution of growth in a representative slice of the internal carotid artery. Growth multiplier, *top*, maximum principal stresses in the adventitia, middle, and maximum principal stresses in the media, *bottom* at 5, 15, 40, and 100 days of hypertension

verged quadratically within a few iterations both locally and globally. The simulations of the circular arterial cross sections finished within a few minutes; the simulations of the human carotid artery finished within a few hours.

We have shown that our model is capable of simulating hypertensive growth in arterial tissue. In particular, we have focused on growth-induced smooth muscle cell hypertrophy. We have assumed that when subjected to mechanical stimuli, smooth muscle cells thicken in the radial direction, while their length remains virtually unchanged [25]. After comparing the two most common mechanical stimuli for growth, stress and strain, we have decided to choose the local smooth muscle cell stretch as the stimulus for smooth muscle cell thickening. The resulting mathematical model allows us to explore how microstructural changes on the smooth muscle cell level translate into a macrostructural thickening of the arterial wall. This is conceptually similar to studying how microstructural changes of heart muscle cells translate into a macroscopic thickening of the ventricular wall in cardiac hypertension [55]. While microstructural changes in cardiac muscle cells [25] and skeletal muscle cells [70] have been attributed to sarcomerogenesis, the creation and deposition of new sarcomere units within the cell, microstructural changes in smooth muscle cells are far more complex and less well documented.

Our simulations display an excellent qualitative and quantitative agreement with experimental findings, both in terms of thickening and growth rates [16]. To demonstrate the potential of the proposed approach, we have shown the finite element simulation of a real patient-specific carotid geometry. Cerebral arteries are an object of intense investigation, since they are at high risk of uncontrolled growth, aneurysm formation [3,66], and rupture [69]. Our results indicate a homogeneous growth throughout the media along the entire carotid length. Only small portions of the carotid bifurcation displayed slightly elevated growth. While previous studies have mainly modeled the growing arterial wall as a single-layer system [28,41], here, we have modeled the media

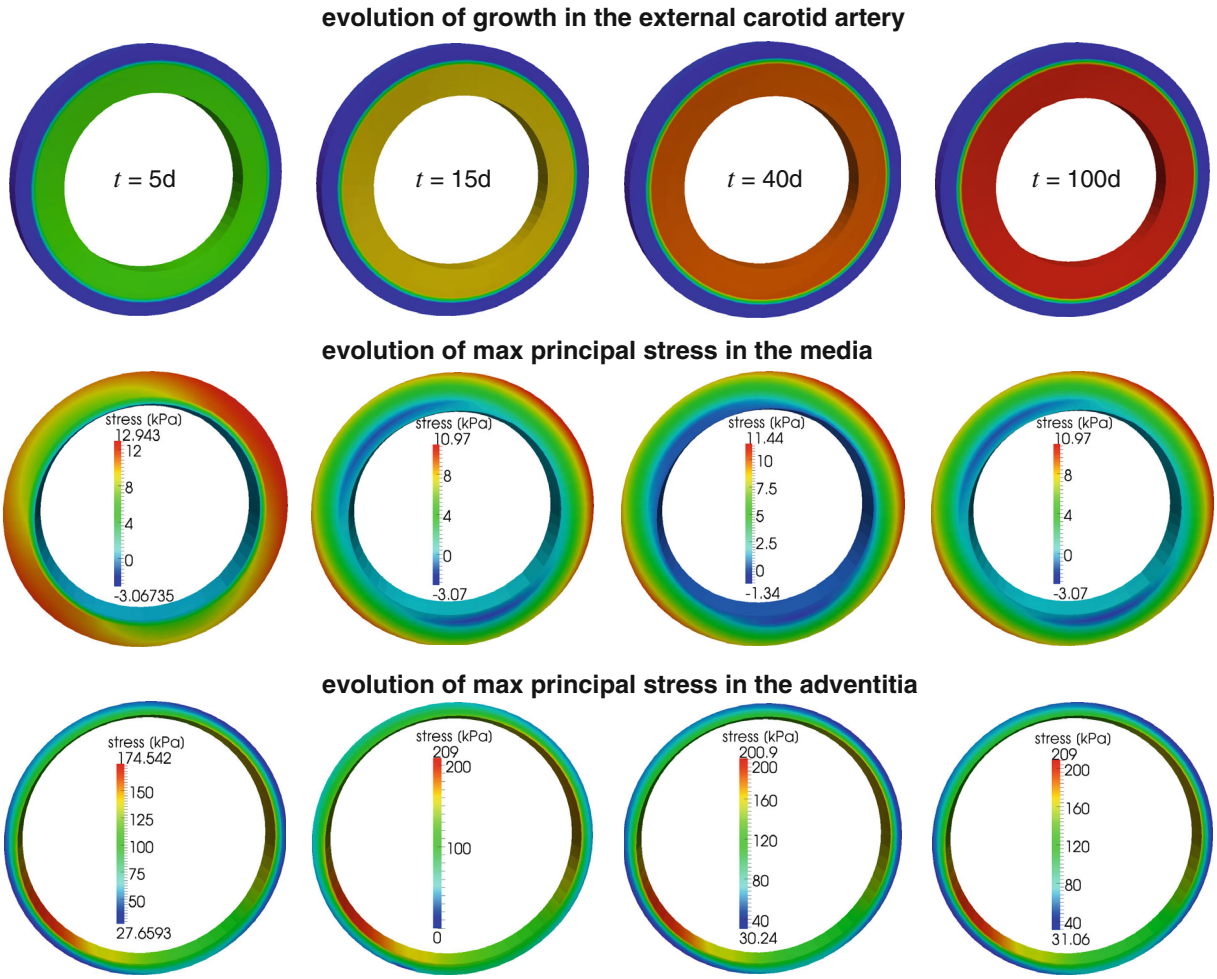

Fig. 14 Spatio-temporal evolution of growth in a representative slice of the external carotid artery. Growth multiplier, *top*, maximum principal stresses in the adventitia, middle, and maximum principal stresses in the media, *bottom* at 5, 15, 40, and 100 days of hypertension

and the adventitia as distinct layers with distinct mechanical properties [30]. This approach raises an interesting question related to the stress distribution. Stresses in the media decrease due to the radial growth of smooth muscle cells. This is a well-accepted mechanism in the adaptation of biological tissue. Smooth muscle cells respond, both acutely and chronically, to hypertension with the goal to bring the wall stress back to its physiological baseline state. Various interconnected mechanotransduction pathways in the cells are responsible for sensing the underlying mechanical stimuli [59,71]. In particular, smooth muscle cells are known to sense stretch in the extracellular matrix. Since smooth muscle cells are mainly present in the media and not in the adventitia, we have assumed that the medial layer grows, while the adventitial layer remains purely elastic. Accordingly, the stresses in the adventitia increase up to a 20–30 %, caused by combined effects of the elevated pressure and the growth of the media. These results reflect the general understanding that the adventitia acts as a protective outer layer.

Despite these promising first results, we would like to address a few fundamental limitations of the current approach. First, our current model is based on purely passive baseline elasticity. Smooth muscle cells display an important active response, the myogenic tone, which allows the arterial wall to contract or expand acutely to maintain a baseline lumen [62]. Our arterial model would improve by the inclusion of this feature, although, up to date, only a few computational models of myogenic tone are available in literature [4,11]. The underlying stimuli for growth could possibly include this basal tone. However, myogenic tone is a response to the overstretch of the smooth muscle cells, which we utilize as stimulus in our current model. We expect that the additional inclusion of basal tone could quantitatively scale our current growth response, but it would not qualitatively modify the growth response overall. Second, our current evolution equation for growth pre-imposes both the growth level and its rate. Its constitutive parameters could be calibrated experimentally to describe specific arteries and other car-

diovascular tissues. At this point though, they lack of a real physiological interpretation. The challenge to tie the parameters to mechanotransduction pathways in arterial cells and tissue introduces an additional limitation. Experiments are usually performed in the normotensive state and in the final hypertensive state, but not in longitudinal studies to explore the transition between the two. Accordingly, most reported experiments do not allow us to calibrate our rate parameters. Moreover, experimental characterizations display huge variations across different species, across different arteries from the same species, and even across different specimen from the same artery.

In summary, we have adopted a canonical framework for volumetric growth to simulate hypertensive thickening of the human carotid artery. Our model makes a first attempt to link the key kinematic variable of growth, the macroscopic growth tensor, to microstructural changes in smooth muscle cell size. The characterization of growth in terms of microstructural variables such as cell size and cell orientation smoothly integrates the multiscale nature of the living system into the mathematical model. Hypertensive arterial wall thickening is a critical medical condition since it may lead to decreases blood flow and other related complications. Computational models like ours can help to understand the underlying mechanochemical processes and provide a framework for biological and clinical researchers to jointly enhance the pharmagolocial or surgical management of hypertension.

References

1. Ambrosi D, Ateshian GA, Arruda EM, Cowin SC, Dumais J, Goriely A, Holzapfel GA, Humphrey JD, Kemkemer R, Kuhl E, Olberding JE, Taber LA, Garikipati K (2011) Perspectives on biological growth and remodeling. J Mech Phys Solids 59:863–883
2. Ateshian GA (2007) On the theory of reactive mixtures for modeling biological growth. Biomech Model Mechanbio 6:423–445
3. Bazilevs Y, Hsu MC, Zhang Y, Wang W, Liang X, Kvamsdal T, Brekken R, Isaken JG (2010) A fully-coupled fluid–structure interaction simulation of cerebral aneurysms. Comput Metods Appl Mech Eng 46:3–16
4. Böl M, Schmitz A, Nowak G, Siebert T (2012) A three-dimensional chemo-mechanical continuum model for smooth muscle contraction. J Mech Behav Biomed Mater 13:215–229
5. Boutouyrie P, Bussy C, Lacolley P, Girerd X, Laloux B, Laurent S (1999) Association between local pulse pressure, mean blood pressure, and large-artery remodeling. Circulation 100:1387–1393
6. Brayden JE, Nelson MT (1992) Regulation of arterial tone by activation of calcium-dependent potassium channels. Science 256:532–535
7. Buganza Tepole A, Ploch CJ, Wong J, Gosain AK, Kuhl E (2011) Growing skin: a computational model for skin expansion in reconstructive surgery. J Mech Phys Solids 59:2177–2190
8. Cardamone L, Valentin A, Eberth JF, Humphrey JD (2010) Modelling carotid artery adaptations to dynamic alterations in pressure and flow over the cardiac cycle. Math Med Biol 27:343–371
9. Davis MJ, Hill MA (1999) Signaling mechanisms underlying the vascular myogenic response. Physiol Rev 79:387–423
10. Eberth JF, Popovic N, Gresham VC, Wilson E, Humphrey JD (2010) Time course of carotid artery growth and remodeling in response to altered pulsatility. Am J Phys Heart Circ Phys 299:H1875–H1883
11. Famaey N, vanSloten J, Kuhl E (2013) A three-constituent damage model for arterial clamping in computer-assisted surgery. Biomech Model Mechanbio 12:123–136
12. Feihl F, Liaudet L, Levy BI, Waeber B (2008) Hypertension and microvascular remodelling. Cardiovasc Res 78:274–285
13. Figueroa CA, Baek S, Taylor CA, Humphrey JD (2009) A computational framework for fluid-solid-growth modeling in cardiovascular simulations. Comput Methods Appl Mech Eng 198:3583–3602
14. Flory PJ (1961) Thermodynamic relations for high elastic materials. Trans Faraday Soc 57:829–838
15. Folkow B, Grimby G, Thulesius O (1958) Adaptive structural changes of the vascular walls in hypertension and their relation to the control of the peripheral resistance. Acta Physiol Scand 44:255–272
16. Fridez P, Makino A, Kakoi D, Miyazaki H, Meister JJ, Hayashi K, Stergiopulos N (2002) Adaptation of conduit artery vascular smooth muscle tone to induced hypertension. Ann Biomed Eng 30:905–916
17. Fung YC, Liu S (1989) Change of residual strains in arteries due to hypertrophy caused by aortic constriction. Circ Res 65:1340–1349
18. Ganghoffer JF (2010) Mechanical modeling of growth considering domain variation. Part II: volumetric and surface growth involving Eshelby tensors. J Mech Phys Solids 58:1434–1459
19. Garcia A (2012) Experimental and numerical framework for modelling vascular diseases and medical devices. PhD thesis, University of Zaragoza, Spain
20. Gasser TC, Holzapfel GA (2002) A rate-independent elastoplastic constitutive model for biological fiber-reinforced composites at finite strains. Comput Methods Appl Mech Eng 29:340–360
21. Gasser TC, Ogden RW, Holzapfel GA (2006) Hyperelastic modeling of arterial layers with distributed collagen fibre orientations. J R Soc Interface 3:15–35
22. Gleason RL, Humphrey JD (2004) A mixture model of arterial growth and remodeling in hypertension: altered muscle tone and tissue turnover. J Vasc Res 41:352–363
23. Gleason RL, Humphrey JD (2005) Effects of a sustained extension on arterial growth and remodeling: a theoretical study. J Biomech 38:1255–1261
24. Göktepe S, Abilez OJ, Kuhl E (2010) A generic approach towards finite growth with examples of athlete's heart, cardiac dilation, and cardiac wall thickening. J Mech Phys Solids 58:1661–1680
25. Göktepe S, Abilez OJ, Parker KK, Kuhl E (2010) A multiscale model for eccentric and concentric cardiac growth through sarcomerogenesis. J Theor Biol 265:433–442
26. Goriely A, BenAmar M (2007) On the definition and modeling of incremental, cumulative, and continuous growth laws in morphoelasticity. Biomech Model Mechanobio 6:289–296
27. Haga JH, Li YSJ, Chien S (2007) Molecular basis of the effects of mechanical stretch on vascular smooth muscle cells. J Biomech 40:947–960
28. Himpel G, Kuhl E, Menzel A, Steinmann P (2005) Computational modelling of isotropic multiplicative growth. CMES Comp Model Eng Sci 8:119–134
29. Holzapfel GA (2000) Nonlinear solid mechanics: a continuum approach for engineering. Wiley, New York
30. Holzapfel GA, Gasser TC, Ogden RW (2000) A new constitutive framework for arterial wall mechanics and a comparative study of material models. J Elast 61:1–48
31. Humphrey JD, Rajagopal KR (2002) A constrained mixture model for growth and remodeling of soft tissues. Math Models Methods Appl Sci 12:407–430

32. Humphrey JD, Rajagopal KR (2003) A constrained mixture model for arterial adaptations to a sustained step change in blood flow. Biomech Model Mechanbio 2:109–126
33. Humphrey JD (2009) Need for a continuum biochemomechanical theory of soft tissue and cellular growth and remodeling. Biomechanical modelling at the molecular, cellular and tissue levels. Springer, Vienna
34. Humphrey JD, Holzapfel GA (2012) Mechanics, mechanobiology, and modeling of human abdominal aorta and aneurysms. J Biomech 45:805–814
35. Imatani S, Maugin GA (2002) A constitutive model for material growth and its application to three-dimensional finite element analysis. Mech Res Commun 29:477–483
36. Klepach D, Lee LC, Wenk JF, Ratcliffe MB, Zohdi TI, Navia JA, Kassab GS, Kuhl E, Guccione JM (2012) Growth and remodeling of the left ventricle. Mech Res Commun 42:134–141
37. Klisch SM, Sah RL, Hoger A (2005) A cartilage growth mixture model for infinitesimal strains: solutions of boundary-value problems related to in vitro growth experiments. Biomech Model Mechanbio 3:209–223
38. Kuhl E, Menzel A, Steinmann P (2003) Computational modeling of growth. Comput Methods Appl Mech Eng 32:71–88
39. Kuhl E, Steinmann P (2003) Theory and numerics of geometrically non-linear open system mechanics. Int J Numer Meth Eng 58:1593–1615
40. Kuhl E, Steinmann P (2003) Mass- and volume-specific views on thermodynamics for open systems. Proc R Soc Lond 459:2547–2568
41. Kuhl E, Maas R, Himpel G, Menzel A (2007) Computational modeling of arterial wall growth. Biomech Model Mechanbio 6:321–331
42. Kuhl E, Holzapfel GA (2007) A continuum model for remodeling in living structures. J Mater Sci 42:8811–8823
43. Lee EH (1969) Elastic–plastic deformation at finite strains. J Appl Mech 36:1–6
44. Lubarda VA, Hoger A (2002) On the mechanics of solids with a growing mass. Int J Solids Struct 39:4627–4664
45. Marsden JE, Hughes TJR (1994) Mathematical foundations of elasticity. Dover Publications, Prentice Hall
46. Menzel A (2004) Modelling of anisotropic growth in biological tissues. Biomech Model Mechanobio 3:147–171
47. Menzel A (2007) A fibre reorientation model for orthotropic multiplicative growth. Biomech Model Mechanobio 6:303–320
48. Menzel A, Kuhl E (2012) Frontiers in growth and remodeling. Mech Res Commun 42:1–14
49. Mulvany MJ, Aalkjaer C (1990) Structure and function of small arteries. Physiol Rev 70:921–961
50. O'Connell MK, Murthy S, Phan S, Xu C, Buchanan J, Spilker R, Dalman RL, Zarins CK, Denk W, Taylor CA (2008) The three-dimensional micro- and nanostructure of the aortic medial lamellar unit measured using 3d confocal and electron microscopy imaging. Matrix Biol 27:171–181
51. Osol G (1995) Mechanotransduction by vascular smooth muscle. J Vasc Res 32:275–292
52. Owens GK (1989) Control of hypertrophic versus hyperplastic growth of vascular smooth-muscle cells. Am J Physiol 257:H1755–H1765
53. Owens GK, Schwartz SM (1983) Vascular smooth-muscle cell hypertrophy and hyperploidy in the Goldblatt hypertensive rat. Circ Res 53:491–501
54. Owens GK, Rabinovitch PS, Schwartz SM (1981) Smooth-muscle cell hypertrophy versus hyperplasia in hypertension. Proc Nat Acad Sci 78:7759–7763
55. Rausch M, Dam A, Göktepe S, Abilez OJ, Kuhl E (2011) Computational modeling of growth: systemic and pulmonary hypertension in the heart. Biomech Model Mechanobio 10:799–811
56. Rausch M, Kuhl E (2013) On the effect of prestrain and residual stress in thin biological membranes. J Mech Phys Solids 61:1955–1969
57. Rodriguez EK, Hoger A, McCulloch AD (1994) Stress-dependent finite growth in soft elastic tissues. J Biomech 27:455–467
58. Rodriguez J, Goicolea JM, Gabaldon F (2007) A volumetric model for growth of arterial walls with arbitrary geometry and loads. J Biomech 40:961–971
59. Saez P, Pena E, Martinez M, Kuhl E (2013) Mathematical modeling of collagen turnover in biological tissue. J Math Biol 67:1765–1793
60. Saez P, Pena E, Martinez M (2013) On the microstructural modeling of patient-specific human carotid artery. (in press)
61. Schofield I, Malik R, Izzard A, Austin C, Heagerty A (2002) Vascular structural and functional changes in type 2 diabetes mellitus: evidence for the roles of abnormal myogenic responsiveness and dyslipidemia. Circulation 106:3037–3043
62. Schubert R, Mulvany MJ (1999) The myogenic response: established facts and attractive hypotheses. Clin Sci 96:313–326
63. Skalak R, Dasgupta G, Moss M, Otten E, Dullemeijer P, Vilmann H (1982) Analytical description of growth. J Theor Biol 94:555–577
64. Sommer G, Holzapfel GA (2012) 3d constitutive modeling of the biaxial mechanical response of intact and layer-dissected human carotid arteries. J Mech Behav Biomed 5:116–128
65. Taber LA (1995) Biomechanics of growth, remodeling, and morphogenesis. Appl Mech Rev 48:487–545
66. Takizawa K, Schjodt K, Puntel A, Kostov N, Tezduyar TE (2012) Patient-specific computer modeling of blood flow in cerebral arteries with aneurysm and stent. Comput Methods Appl Mech Eng 50:675–686
67. Valentin A, Humphrey JD, Holzapfel GA (2013) A finite element-based constrained mixture implementation for arterial growth, remodeling, and adaptation: theory and numerical verification. Int J Numer Methods Biomed Eng 29:822–849
68. Wiener J, Loud AV, Giacomelli F, Anversa P (1977) Morphometric analysis of hypertension-induced hypertrophy of rat thoracic aorta. Am J Pathol 88:619–633
69. Zohdi TI, Holzapfel GA, Berger SA (2004) A phenomenological model for atherosclerotic plaque growth and rupture. J Theor Biol 227:437–443
70. Zöllner AM, Abilez OJ, Böl M, Kuhl E (2012) Stretching skeletal muscle: chronic muscle lengthening through sarcomerogenesis. PLoS One 7:e45661
71. Zöllner AM, Buganza-Tepole A, Kuhl E (2012) On the biomechanics and mechanobiology of growing skin. J Theor Biol 297:166–175
72. Zöllner AM, Holland MA, Honda KS, Gosain AK, Kuhl E (2013) Growth on demand: reviewing the mechanobiology of stretched skin. J Mech Behav Biomed Mater 28:495–509